Universiteit Leiden
The Netherlands

Hybrid Josephson junctions and their qubit applications
Vakhtel, T.

Chapter 3

Tunneling of fluxons via a Josephson resonant level

3.1 Introduction

The inductively shunted Josephson junction plays an important role in the field of superconducting quantum devices [143, 144]. The inductive link changes the topology of the circuit from that of an island to that of a loop, removing the $2e$ charge quantization associated with a superconducting island. The charge sensitivity of the device is exchanged for its flux sensitivity [27], which is exploited in the design and operation of the fluxonium qubit [28, 30–33]. Furthermore, a large shunting inductance suppresses the sensitivity to flux noise, as recently demonstrated in the blochnium qubit [34]. For this reason, the inductive shunt is a common feature of noise-protected qubit designs [111].

The minimal circuit that models this class of superconducting devices is simple: it consists of an inductor, a capacitor and a Josephson element connected in parallel [Fig. 3.1(a)]. The inductor and the Josephson junction form a loop through which an applied magnetic flux Φ is threaded. The circuit supports persistent current states, also known as *fluxons*, in which the superconducting phase winds by an integer multiple m of 2π when circling the loop [94]. Fluxons are coupled by quantum phase slips occurring at the Josephson junction [1], which change m by an integer Δm (see Fig. 3.2).

---

[1]In principle, phase slips may also occur at other points in the loop, through the inductor. We neglect this possibility, which is analyzed in Ref. [89]
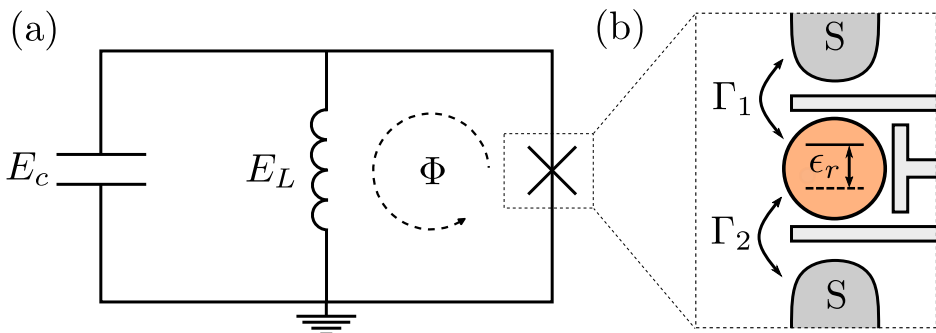
Figure 3.1. (a) Circuit of the inductively shunted Josephson junction. (b) A junction realized by a resonant level with a tunable energy ϵ_r and Cooper pair tunneling rates Γ_1 and Γ_2.

In a typical Josephson element, e.g. in a tunnel junction, the amplitude of 2π quantum phase slips ($\Delta m = 1$) is much larger than that of 4π quantum phase slips ($\Delta m = 2$). However, if Cooper pair tunneling across the Josephson element is resonant – a type of weak link we call the Josephson resonant level – 2π quantum phase slips are suppressed [22, 114–116] and 4π quantum phase slips become the dominant coupling between fluxons. The bifluxon qubit proposal [7] achieves resonant tunneling using as a Josephson element a series of two (almost) identical tunnel junctions separated by a small superconducting island tuned (close) to a charge degeneracy point. Alternatively, resonant tunneling can also occur in a semiconductor junction, via an isolated energy level forming in a quantum dot [117, 118, 121], as represented in Fig. 3.1(b). In the latter system, experiments have demonstrated the drastic suppression of 2π quantum phase slips close to resonance [16, 17], but not yet the occurrence of the regime dominated by 4π quantum phase slips [22].

In this chapter, motivated by these experimental developments, we study in detail the energy spectrum of an inductively shunted junction with a Josephson coupling mediated by a single energy level [Fig. 3.1(b)]. We focus on the avoided crossings between energy levels directly connected to the quantum phase slip amplitudes, and measurable via microwave spectroscopy. We provide analytical expressions, backed by numerics, that capture the entire crossover between 2π- and 4π-dominated regimes near the resonance, as well as the regime away from resonance.

We also show that, when the inductive energy of the loop becomes much smaller than the Josephson plasma frequency, the circuit is well

described by a low-energy theory dual to that of a topological supercon-
ducting island. The duality we uncover extends a known duality between
a superconducting loop and a superconducting island [86]. It does so by
including an additional degree of freedom: the *fluxon parity* of the loop
(i.e. the parity of m), which we show to be dual to the *fermion par-
ity* of the island. Similar to fermion parity states encoded non-locally
in Majorana zero modes, states with opposite fluxon parity have disjoint
support in phase and provide a two-fold quasi-degeneracy to the energy
spectrum; thus, they become an attractive degree of freedom to encode
qubit states [7, 145]. We discuss the implications of our findings for the
design of protected qubits [111, 145] in the concluding section.

3.2 Model

Given a capacitance C and an inductance L, the inductively shunted junc-
tion of Fig. 3.1(a) is described by the quantum Hamiltonian [27]:

$$\hat{H} = 4E_C\hat{n}^2 + \tfrac{1}{2}E_L(\hat{\phi} + \phi_{\text{ext}})^2 + V(\hat{\phi})\,, \qquad (3.1)$$

where $E_C = e^2/2C$ and $E_L = (\Phi_0/2\pi)^2/L$. The parameter $\phi_{\text{ext}} = 2\pi\Phi/\Phi_0$
gives the applied flux Φ through the inductive loop in units of the flux
quantum $\Phi_0 = h/2e$. The Cooper pair number $\hat{n}$ and phase $\hat{\phi}$ are conju-
gate variables satisfying $[\hat{\phi}, \hat{n}] = i$.

The potential term $V(\hat{\phi})$ gives the Josephson energy, which for a tunnel
junction would be the familiar $-E_J\cos\hat{\phi}$. For the case in which Joseph-
son coupling is mediated by an isolated energy level, as in Fig. 3.1(b), a
minimal model for the potential is:

$$V(\hat{\phi}) = -\Gamma\,\cos(\hat{\phi}/2)\tau_x - \delta\Gamma\,\sin(\hat{\phi}/2)\tau_y - \epsilon_r\tau_z\,. \qquad (3.2)$$

Here, the Pauli matrices τ_x, τ_y, τ_z act on the two-level system correspond-
ing to the resonant level being empty or doubly occupied; $\Gamma = \Gamma_1 + \Gamma_2$
and $\delta\Gamma = \Gamma_1 - \Gamma_2$ are the sum and difference of the $2e$ tunneling rates Γ_1
and Γ_2 between the two leads and the resonant level; and finally ϵ_r is the
energy of the resonant level [see Fig. 3.1(b)]. This model for the Joseph-
son resonant level has been discussed in Refs. [18, 19, 22]. Among other
things, these works discuss the role of a charging energy of the resonant
level, as well as the effect of additional transport channels and the contin-
uum part of the density of states; all elements which we do not include in
our work for simplicity.
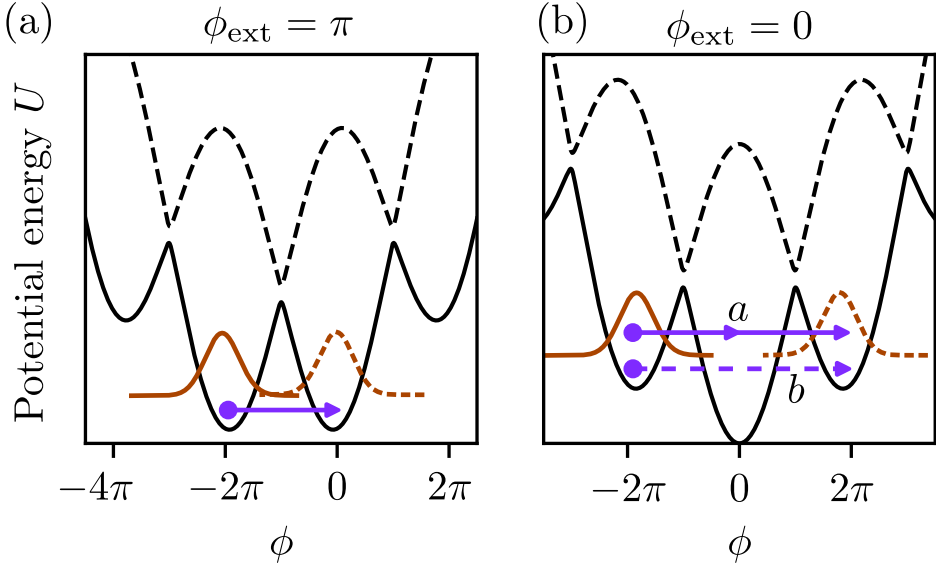
Figure 3.2. Potential landscape of the model of Eq. (3.1). We depict the two branches of the potential energy $U(\phi) = \frac{1}{2}E_L(\phi + \phi_{\text{ext}})^2 \pm E_A(\phi)$. (a) When the external flux is equal to half a flux quantum, fluxons are localized around the Josephson potential minima at $\phi = 0, 2\pi$ (wave functions shown in orange). Fluxons can tunnel between the minima via a 2π quantum phase slip (purple arrow). (b) When the external flux is zero, fluxons localized around $\phi = \pm 2\pi$ can tunnel via 4π quantum phase slips. Because of the second branch of the potential, the 4π quantum phase slips can follow two interfering paths labeled a and b (solid and dashed arrows), as described in the text.

The potential in Eq. (3.2) also applies to the bifluxon circuit deep in the charging regime of the middle island [7], but parameters have a slightly different meaning: Γ_1 and Γ_2 are Josepshon energies of two tunnel junctions, and ϵ_r is the energy difference between two even-parity charge states of the superconducting island.

Fluxonium devices are typically operated in a parameter regime such that there is approximately one bound state in each of the local minima of the modulated potential of Eq. (3.1) [28]. These bound states are fluxons with a parabolic energy dispersion $\approx \frac{1}{2}E_L(2\pi m + \phi_{\text{ext}})^2$ [see Fig. 3.3(a)], and become degenerate for particular values of ϕ_{ext}. At the degeneracy points, quantum phase slips create coherent superpositions of fluxons.

In particular, at $\phi_{\text{ext}} = \pi$ the potential landscape is a degenerate double well for fluxons with $m = 0$ and $m = -1$, which couple via 2π

quantum phase slips [see Fig. 3.2(a)]. At $\phi_{\text{ext}} = 0$, instead, fluxons with $m = \pm 1$ occupy degenerate minima symmetrically placed around $\phi = 0$, and are coupled by 4π quantum phase slips [see Fig. 3.2(b)]. When $V(\phi) = -E_J \cos \phi$, the 4π quantum phase slips have a much smaller amplitude than 2π ones, since they are a higher-order process involving two 2π-slips [27].

This is not necessarily the case for the Josephson resonant level [Eq. (3.2)], because of the presence of a second branch corresponding to an excited Andreev pair in the junction [146]. Indeed, the matrix-valued potential $V(\hat{\phi})$ has eigenvalues $\pm E_A$, with

$$E_A = \Gamma_A \sqrt{\cos^2(\phi/2) + |r|^2 \sin^2(\phi/2)}\,, \qquad (3.3)$$

where

$$\Gamma_A = \sqrt{\Gamma^2 + \epsilon_r^2}\,, \qquad (3.4)$$

and

$$r = \frac{\epsilon_r + i\delta\Gamma}{\Gamma_A} \qquad (3.5)$$

is the reflection amplitude of the junction.

The excited energy branch $+E_A$ is shown as a black dashed line in Fig. 3.2(a,b). The relevant feature of Eq. (3.3) is an avoided crossing of magnitude $|r|\,\Gamma_A$ at $\phi = \pm\pi, \pm 3\pi, \ldots$. In the next section we show that in the limit $r \to 0$, when the branches cross, the amplitude of 2π phase slips vanishes. The system thus enters the regime in which 4π phase slips are dominant.

3.3   Wentzel–Kramers–Brillouin (WKB) analysis

An observable consequence of quantum phase slips are avoided crossings in the flux dependence of the energy spectrum of the circuit, see Fig. 3.3. There, $\Delta_{2\pi}$ is the splitting of the crossing between states with $m = 0$ and $m = -1$ at $\phi_{\text{ext}} = \pi$; it originates from 2π phase slips. $\Delta_{4\pi}$ is the splitting of the crossing between states with $m = -1$ and $m = 1$ at $\phi_{\text{ext}} = 0$; it originates from 4π phase slips. The magnitude of these avoided crossings can be computed using the WKB method [129], with calculations similar to the one described in detail in Ref. [22]. One must perform separate calculations to determine $\Delta_{2\pi}$ and $\Delta_{4\pi}$, respectively using the two potential landscapes at $\phi_{\text{ext}} = \pi$ and $\phi_{\text{ext}} = 0$ [Fig. 3.2(a,b)]. In both
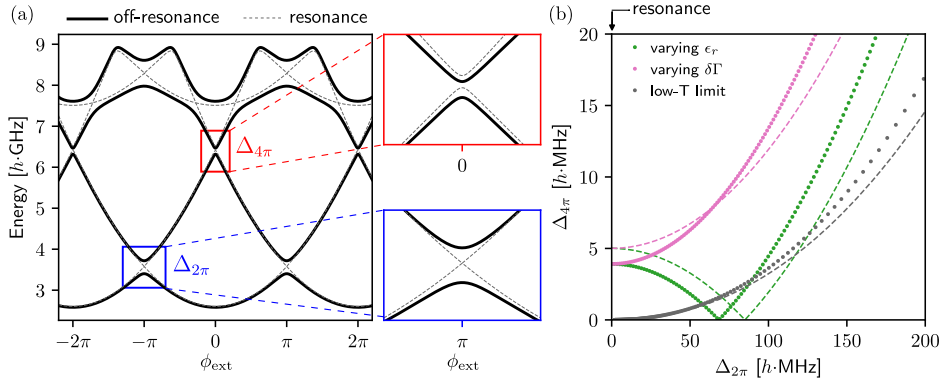
Figure 3.3. (a) Energy spectrum as a function of flux, ϕ_{ext}. The blue and red insets zoom in on the avoided crossings due to 2π and 4π quantum phase slips respectively (the vertical span of the insets is 1 GHz). The energies are computed numerically from Eq. (3.1), with $E_C/h = 2.5$ GHz, $E_L/h = 0.25$ GHz, $\Gamma/h = 5$ GHz, $\delta\Gamma/h = \epsilon_r = 0.5$ GHz. These parameters correspond to a reflection coefficient $|r| = 0.14$. The dashed gray lines illustrate the resonant case in which $\epsilon_r = \delta\Gamma = 0$ and so $r = 0$. (b) Comparison of the avoided crossings $\Delta_{2\pi}$ and $\Delta_{4\pi}$ when sweeping system parameters. For all curves, we fix $E_C/h = 2.5$ GHz and $E_L/h = 0.25$ GHz. The pink and green data show results obtained approaching resonance in two different ways. In both cases we set $\Gamma/h = 10$ GHz. In green, ϵ_r/h is varied between 0 and 1 GHz, with $\delta\Gamma = 0$. In pink, $\delta\Gamma/h$ is varied instead between 0 and 1 GHz, with $\epsilon_r = 0$. For both curves, $|r| \approx 0.1$ on the right side of the plot, and tends towards 0 on the left side of the plot, where $\delta\Gamma = \epsilon_r = 0$ and $\Delta_{2\pi}$ vanishes. Dots are computed numerically by diagonalizing Eq. (3.1), while dashed lines are obtained from the WKB result of Eqs. (3.6) and (3.9). The grey dots show the low-transparency scaling obtained from numerical diagonalization of Eq. (3.1) with $V(\hat{\phi}) = -E_J \cos \hat{\phi}$, varying E_J/h between 10 and 40 GHz. The dashed line corresponds to the $T \ll 1$ limit of Eqs. (3.6) and (3.9), with the correspondence $E_J = \Gamma_A T/4$.

cases, the presence of a second branch of the potential crucially modifies the WKB tunneling amplitude under the barrier separating different local minima [22, 114–116, 136].

In this section, we discuss the implications of this fact using a WKB calculation appropriate for the parameter regime typical of fluxonium qubits, in particular with respect to the value of E_L. In the next section, the results are generalized to arbitrarily low values of the inductive energy.

For the 2π quantum phase slips at $\phi_{\text{ext}} = \pi$, under validity conditions

discussed at the end of the Section, one obtains

$$\Delta_{2\pi} = w(r)\,\omega_p \left(\frac{b_0^2 \omega_p}{2\pi E_C} \right)^{1/2} \exp\left(-b_1 \frac{\omega_p}{E_C} + b_2 \frac{E_L}{\omega_p} \right). \qquad (3.6)$$

where

$$\omega_p = \sqrt{2T\Gamma_A E_C}\,, \quad T = 1 - |r|^2\,, \qquad (3.7)$$

and b_0, b_1, b_2 are numerical coefficients which depend smoothly on the transmission probability T. They are given in Appendix 3.6. The pre-factor $w(r)$ is given by

$$w = \sqrt{\frac{2\pi}{\lambda}} \frac{e^{-\lambda}\lambda^\lambda}{\Gamma(\lambda)}\,, \quad \lambda = \frac{|r|^2}{4} \frac{\Gamma_A}{\Gamma} \sqrt{\frac{\Gamma_A}{E_C}}. \qquad (3.8)$$

with $\Gamma(\lambda)$ the gamma function evaluated at λ, not to be confused with tunneling rates. The amplitude w vanishes when $r \to 0$, making the fluxon bound states degenerate at $\phi_{\text{ext}} = \pi$. The parameter λ sets the scale for the crossover into the degenerate regime: the suppression of $\Delta_{2\pi}$ takes place when $\lambda \ll 1$, namely when $|r|^2 \ll \sqrt{E_C/\Gamma}$, while $w \approx 1$ in the opposite limit $\lambda \gg 1$. The mechanism behind the suppression is the imaginary-time Landau-Zener transition across the avoided crossing [114].

The WKB calculation of $\Delta_{4\pi}$ is more delicate, because there are two tunneling paths between the minima at $\phi = \pm 2\pi$, labeled a and b in Fig. 3.2(b). They differ by the branch of the potential that they take between the two avoided crossings at $\phi = \pm\pi$. Path a takes place via the lower branch of the potential. It consists of the sequence of two 2π phase slips, passing through a classically available region around $\phi = 0$. Path b, instead, takes place via the excited branch of the potential and passes through a single 4π-wide tunneling barrier.

Notably, the two contributions interfere. The interference phase is that of the reflection amplitude $r = |r|\,e^{i\alpha}$, which distinguishes the path going through the avoided crossings from the one which does not. The sensitivity of energy levels to the phase acquired at the avoided crossing is akin to the Landau-Zener-Stückelberg interference [147]. The final result for the energy splitting takes the form

$$\Delta_{4\pi} = \sqrt{\Delta_a^2 + \Delta_b^2 - 2\,\Delta_a\,\Delta_b\,\cos(2\alpha)}. \qquad (3.9)$$

Here, Δ_a is the contribution due to the sequence of two 2π phase slips. It takes the form:

$$\Delta_a = \frac{\Delta_{2\pi}^2}{4\pi^2 E_L} \left(\frac{b_0^2 \omega_p}{2E_C} \right)^{2\pi^2 E_L/\omega_p} \tag{3.10}$$

where $\Delta_{2\pi}$ is the same as given in Eq. (3.6). Note that this contribution vanishes when $r \to 0$. On the other hand, Δ_b is the amplitude of a direct 4π quantum phase slip. It does not vanish at resonance, and is given by

$$\Delta_b = \omega_p \left(\frac{b_0^2 \omega_p}{2\pi E_C} \right)^{1/2} \exp \left(-b_3 \sqrt{\frac{\Gamma_A}{E_C}} + b_4 \frac{E_L}{\omega_p} + b_5 \right) \tag{3.11}$$

with b_3, b_4, b_5 another three coefficients smoothly depending on T, also given in Appendix 3.6.

The results of Eq. (3.6) and (3.9) are illustrated in Fig. 3.3. The parametric plot of $\Delta_{4\pi}$ versus $\Delta_{2\pi}$ shows that, close to resonance, $\Delta_{2\pi}$ vanishes and $\Delta_{4\pi}$ remains finite. The 4π-dominated regime is approached differently depending on whether the junction is tuned to resonance by varying $\delta\Gamma$ or by varying ϵ_r. When $\delta\Gamma \neq 0$, $\alpha = \pi/2$ in Eq. (3.9), and so Δ_a and Δ_b can never cancel out. When $\epsilon_r \neq 0$, $\alpha = 0$, and so complete cancellation ($\Delta_{4\pi} = 0$) occurs at the value of ϵ_r such that $\Delta_a = \Delta_b$.

Eqs. (3.6) and (3.9) are valid when $E_C \ll \Gamma_A T/4$, $E_L \ll \omega_p$, and $\max(\Delta_{2\pi}, \Delta_{4\pi}) \ll E_L$, and apply only to the splitting of fluxons belonging to the lowest harmonic level in the relevant potential minima. The first condition is required for the validity of the semiclassical WKB approach. The second condition guarantees that we can disregard fluxons originating from the other harmonic levels inside the wells. Finally, the third condition allows us to ignore the presence of the higher-energy minima of the potential energy. The assumed hierarchy of energy scales is in line with experimentally reported parameters of fluxonium devices [28, 148, 149], with better accuracy in the "heavy" regime $E_C \ll \Gamma_A T/4$ [148, 149].

In Eqs. (3.6) and (3.11) we include contributions to the WKB exponent proportional to the small parameter E_L/ω_p. These contributions originate from the lifting of the energy minima of the periodic potential $V(\phi)$, as well as the change in the WKB momentum due to the E_L term. Although they are sub-leading contributions to the WKB integrals, and are subtle to compute, we find that they are important for the agreement with numerical calculations in the parameter regime of the aforementioned experiments, such as the parameters used in Fig. 3.3.
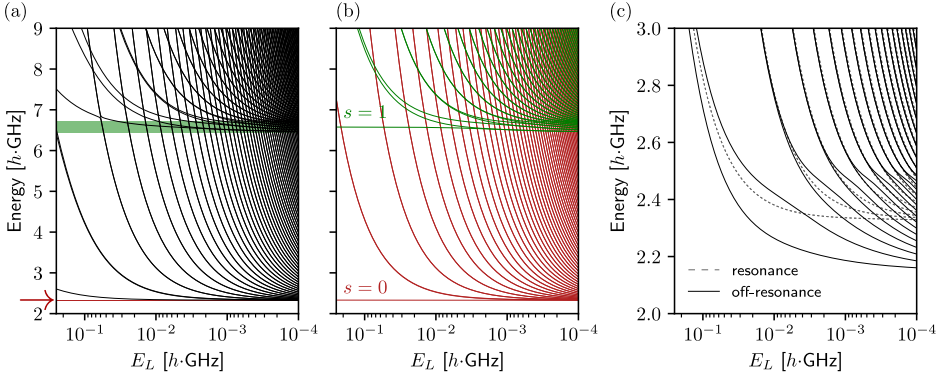
Figure 3.4. Energy spectrum as a function of decreasing inductive energy E_L. (a) Energy levels determined from direct numerical diagonalization of Eq. (3.1); the parameters are $E_C/h = 2.5$ GHz, $\Gamma/h = 5$ GHz, $\phi_{\text{ext}} = 0$, $\epsilon_r/h = 10$ MHz and $\delta\Gamma = 0$, corresponding to $r \approx 0.002$, very close to resonance. As $E_L \to 0$, the energy levels tend to fill the areas shaded in red and green. These correspond to the energy bands defined in Eq. (3.15) for $s = 0, 1$. The bandwidth of the $s = 0$ band is barely resolvable at about 16 MHz and so it is also indicated by the red arrow. (b) Result of the numerical diagonalization of the effective Hamiltonian H_s of Eq. (3.18), separately for $s = 0, 1$. The quantum phase slip amplitudes used in the effective Hamiltonian are $A_0 \approx 2.8$ MHz, $B_0 \approx 6.6$ MHz; and $A_1 \approx 7.8$ MHz, $B_1 \approx 133$ MHz. While the effective spectrum in (b) faithfully reproduces the clustering of energy levels into bands, it does not capture avoided crossings in (a) that originate from the inter-band couplings. (c) Low-lying energy levels computed for the $s = 0$ band at $\phi_{\text{ext}} = \pi$ both on resonance ($\delta\Gamma = \epsilon = 0$) and off-resonance ($\delta\Gamma = \epsilon_r = 0.5$ GHz, i.e., $|r| \approx 0.14$). The low-energy effective parameters are $A_0 = 0$ and $B_0 \approx 6.6$ MHz for the resonant case, and $A_0 \approx 160$ MHz and $B_0 \approx 7.3$ MHz for the off-resonant case. The panel illustrates the different degeneracy of energy levels that is observed in the two cases: degenerate doublets in the resonant case split off-resonance due to 2π quantum phase slips.

As long as $E_C \ll \Gamma_A T/4$, Eqs. (3.6) and (3.9) remain valid also in the low-transparency regime $T \ll 1$, away from resonance. In fact, in the limit $T \ll 1$, Eq. (3.6) and (3.9) match exactly the results of an equivalent WKB calculation done with the tunnel junction potential $V(\hat\phi) = -E_J \cos\hat\phi$, provided that one sets $E_J = \Gamma_A T/4$ so that $\omega_p = \sqrt{8E_J E_C}$. In this off-resonant regime one always has $\Delta_{4\pi} \ll \Delta_{2\pi}$, as shown by the gray lines in Fig. 3.3.

3.4 Duality with a topological superconducting island

We now ask what happens to the low energy spectrum when E_L is lowered, so that the assumption $E_L \gg \max(\Delta_{4\pi}, \Delta_{2\pi})$ behind the results from the last section is violated and the discussed eigenstates are delocalized over more minima.

The scaling of the energy spectrum of Eq. (3.1) towards the limit $E_L \to 0$ is shown in Fig. 3.4. In the limit $E_L \ll \omega_p$, as more and more local minima of the potential appear at energies below ω_p, we observe the condensation of bands of narrowly spaced energy levels. We now derive an effective Hamiltonian appropriate to describe this regime, via similar steps as those described in Ref. [27] for the standard fluxonium Hamiltonian. The derivation will establish the duality with the topological superconducting island mentioned in the introduction.

To begin with, when $E_L \ll \omega_p$, it becomes convenient to write the Hamiltonian (3.1) in the eigenbasis of its $E_L \to 0$ limit. The eigenfunctions can be represented in the following way:

$$\Psi_{ns}(\phi) = e^{-in\phi} u_{ns}(\phi) \equiv \langle \phi \mid n, s \rangle. \tag{3.12}$$

Here, s is an integer number that refers to a band index and n is a continuous variable, $n \in [0, 1)$. By substitution into (3.1), the spinor wave functions $u_{ns}(\phi)$ satisfy a transmon-like equation:

$$[4E_C(-i\partial_\phi - n)^2 + V(\phi)]\, u_{ns} = E_s(n)\, u_{ns}, \tag{3.13}$$

with the boundary condition that was derived in Ref. [22]:

$$u_{ns}(\phi + 2\pi) = \tau_z u_{ns}(\phi)\ . \tag{3.14}$$

Note that u_{ns} are defined on the circle $\phi \in [0, 2\pi)$ and, at a fixed n, they form an orthonormal basis with respect to the band index s. This ensures that $\Psi_{ns}(\phi)$, which are functions of a non-compact phase, form an orthonormal basis with different s and n.

This eigenvalue problem was analyzed in Ref. [22], where we showed that the eigenspectrum takes the form:

$$E_s(n) = \epsilon_s + A_s \cos(2\pi n + \alpha_s) + B_s \cos(4\pi n + \beta_s)\,. \tag{3.15}$$

Here, A_s and B_s are the 2π and 4π quantum phase slip tunneling amplitudes for the periodic potential $V(\phi)$, and α_s and β_s are associated phase

shifts. The bands are harmonically spaced, $\epsilon_s \approx \omega_p(s + \frac{1}{2})$, while A_s and B_s are exponentially small in ω_p/E_C. Detailed expressions as a function of E_C, Γ, $\delta\Gamma$ and ϵ_r are derived in Ref. [22] and restated in Appendix 3.7. The simple form above for the energy bands was derived via the WKB method. It is accurate for $E_C \ll \Gamma_A T/4$ and for low-lying bands.

For the lowest band, the parameters A_0 and B_0 are closely connected to the quantities $\Delta_{2\pi}$ and $\Delta_{4\pi}$ computed in the previous section. In particular, A_0 can be identified with the limit $E_L/\omega_p \to 0$ of $\Delta_{2\pi}$ in Eq. (3.6), but the same is not true for B_0, since in Eq. (3.9) the ratio $\Delta_{2\pi}/E_L$ appears as well (i.e., both A_0 and B_0 contribute to $\Delta_{4\pi}$). We have verified numerically that the low-energy spectrum of the $s = 0$ band, discussed in more detail below, matches the expressions for the energy splittings given in Eqs. (3.6) and (3.9). This is true provided E_L is low enough to neglect the sub-leading E_L/ω_p terms in those equations, but large enough so that $E_L \gg \max(\Delta_{2\pi}, \Delta_{4\pi})$ as required in the previous section.

In the basis $|n, s\rangle$, the phase operator is represented as $\hat{\phi} = -i\partial_n - \hat{\Omega}$. It couples different bands only via the connection matrix elements $\Omega_{ss'}$:

$$\langle n, s| \hat{\Omega} |n', s'\rangle = \delta(n - n')\Omega_{ss'}(n)$$
$$\Omega_{ss'}(n) = i \int_0^{2\pi} u_{ns}^\dagger \partial_n u_{ns'} d\phi \tag{3.16}$$

These can be evaluated in the same limit where (3.15) was calculated:

$$\Omega_{ss'}(n) \approx -\left(\frac{8E_C}{\Gamma_A T}\right)^{1/4} \left(\sqrt{s}\delta_{s',s+1} + \sqrt{s+1}\delta_{s',s-1}\right). \tag{3.17}$$

The interband couplings can be neglected for $E_C \ll \Gamma_A T/4$. Therefore, the original Hamiltonian of Eq. (3.1) separates into blocks labelled by the band index s:

$$H_s = \tfrac{1}{2}E_L(-i\partial_n + \phi_{\text{ext}})^2 + E_s(n). \tag{3.18}$$

It must be solved with the periodic boundary conditions $\psi_s(n+1) = \psi_s(n)$. The eigenvalues of this block-diagonal Hamiltonian, shown in the right panel of Fig. 3.4, compare favorably to the numerical solution of the full Hamiltonian, Eq. (3.1), shown in the left panel of Fig. 3.4.

The fluxon states localized around minima $\phi = 2\pi m$ with integer m are related to $|n, s\rangle$ via the Fourier transform:

$$|2\pi m, s\rangle = \int_0^1 dn e^{2\pi i m n} |n, s\rangle. \tag{3.19}$$

It is easy to see that, at resonance, A_s vanishes and the parity of m becomes conserved. With this in mind, we introduce in lieu of $|n, s\rangle$ a new basis $|n, \sigma, s\rangle$ endowed with a spin-like degree of freedom related to the fluxon parity:

$$|n, \uparrow, s\rangle = \frac{|n, s\rangle + |n + 1/2, s\rangle}{\sqrt{2}}, \qquad (3.20)$$

$$|n, \downarrow, s\rangle = \frac{|n, s\rangle - |n + 1/2, s\rangle}{\sqrt{2}}, \qquad (3.21)$$

with $n \in [0, 1/2)$. In terms of these basis states,

$$|2\pi m, s\rangle = \sqrt{2} \int_0^{1/2} dn\, |n, \sigma, s\rangle\, e^{2\pi i m n}, \qquad (3.22)$$

where m is even for $\sigma = \uparrow$ and odd for $\sigma = \downarrow$.

The Hamiltonian H_s in this doubled space reads

$$\begin{aligned} H_s = &\tfrac{1}{2} E_L (i\partial_n - \phi_{\text{ext}})^2 + A_s \sigma_x \cos(2\pi n + \alpha_s) \\ &+ B_s \cos(4\pi n + \beta_s) + \epsilon_s. \end{aligned} \qquad (3.23)$$

The Pauli matrices act on the spin-like degree of freedom and the boundary conditions in the halved Brillouin zone become twisted:

$$\psi_s(n + \tfrac{1}{2}) = \sigma_z \psi_n(n). \qquad (3.24)$$

Although Eq. (3.23) is just a re-writing of Eq. (3.18), it illuminates the fact that the low-energy description is precisely dual to that of a superconducting island shunted to ground by a topological Josephson junction with coupled Majorana zero modes [see Fig. 3.5(a)]. The Hamiltonian of such an island is [140, 150–152]

$$\begin{aligned} H_M = &4E_C (i\partial_\phi - n_g)^2 + E_M\, i\gamma_1 \gamma_2\, \cos(\phi/2) \\ &- E_J \cos\phi. \end{aligned} \qquad (3.25)$$

Here, the first term is the charging energy of the island, n_g is the induced charge in units of $2e$, E_J represent standard Cooper pair tunneling, and the last term represents single-charge tunneling due to the Majorana zero modes γ_1 and γ_2 coupled across the topological junction (the fractional Josephson effect). Note that there are four Majorana zero modes in the model, with γ_0 and γ_1 located on the island and γ_2 and γ_3 located

on the ground plane (see Fig. 3.5). Although only γ_1 and γ_2 appear in the Hamiltonian, the boundary condition for Eq. (3.25) depends on the fermion parity operator of the island $i\gamma_0\gamma_1$:

$$\psi(\phi + 2\pi) = (-1)^p \, \psi(\phi), \qquad (3.26)$$

with $p = (1 - i\gamma_0\gamma_1)/2 = 0$ or 1 if the parity is even or odd. The operator $i\gamma_0\gamma_1$ appearing in the boundary condition anticommutes with $i\gamma_1\gamma_2$ appearing in the Hamiltonian, just like the fluxon parity σ_z entering the boundary condition of Eq. (3.24) anticommutes with σ_x.

As illustrated in Fig. 3.5(a) and (b), the duality is established via the following correspondences: $\phi \leftrightarrow 4\pi n$, $\phi_{\text{ext}} \leftrightarrow 4\pi n_g$, $E_C \leftrightarrow 2\pi^2 E_L$, $E_J \leftrightarrow B_s$, $E_M \leftrightarrow A_s$. The operator $i\gamma_1\gamma_2$ changes the fermion parity of the island, just like the operator σ_x changes the fluxon parity. The phase shifts α_s and β_s can be included in the correspondence by adding a relative phase between the E_M and E_J terms, which could arise for instance in a superconducting quantum interference device (SQUID) configuration. Finally, we note a difference between this duality and the one between the Cooper-pair box and the phase-slip junction discussed by Mooij and Nazarov [86]: in our case, 2π quantum phase slips are dual to charge $1e$ tunneling, rather than $2e$ tunneling. This different mapping means that the duality of Mooij and Nazarov cannot be recovered simply by disregarding 4π phase slips.

It follows from the duality that, in the limit of low E_L, the flux dispersion of the energy levels of the circuit is equivalent to the charge dispersion of the energy levels of a superconducting island governed by Eq. (3.25). The first consequence of the duality is illustrated in Fig. 3.4(c), where we focus on the lowest energy levels of the $s = 0$ band when $\phi_{\text{ext}} = \pi$. In this case, at resonance, fluxon parity provides a two-fold degeneracy to the energy spectrum of the circuit, which is broken by 2π quantum phase slips away from resonance. The flux dispersion of energy levels away from this point is instead shown in Fig. 3.5: when $2\pi^2 E_L \gg B_0$, the circuit is in a "Cooper-pair box regime": the energy levels are essentially given by parabolas with small avoided crossings at degeneracy points [see Fig. 3.5(b)]. On the other hand, when $2\pi^2 E_L \ll B_0$, the circuit is in a "transmon regime" [see Fig. 3.5(c)], characterized by a flattening of the dispersion of energy levels as a function of flux. The spacing between these flat energy levels depends on the value of A_0. If $A_0 = 0$, the energy levels become fluxon-parity degenerate doublets at all values of the flux in the

limit $E_L \to 0$, with a spacing between doublets $\sim \sqrt{E_L B_0}$ [dashed lines in Fig. 3.5(c)]. A finite but small 2π quantum phase slip amplitude splits the doublets by an amount $\approx A_0$ [solid lines in Fig. 3.5(c)].

3.5 Conclusion

The difficulty of measuring directly the 4π-dominated regime occurring at resonance lies in the smallness of 4π quantum phase slips. This was the reason, for instance, that the effect of 4π quantum phase slips was not detected in the transmon experiments of Ref. [16, 17]. The results of Fig. 3.3 show that measuring the 4π-dominated regime should be feasible in circuit with typical fluxonium parameters: $E_C/h = 2.5$ GHz and $E_L/h = 0.25$ GHz. At perfect resonance, when $\Delta_{2\pi}$ vanishes, $\Delta_{4\pi}/h \approx 5$ MHz if $\Gamma/h \approx 5$ GHz: albeit small, splittings of this magnitude have been detected and exploited in heavy fluxonium circuits [148, 153]. Larger values of $\Delta_{4\pi}$ can be obtained by decreasing Γ_A/E_C (somewhat exiting the domain of validity of our WKB results).

The 4π-dominated regime is narrow: with the parameters of Fig. 3.3, one needs $\epsilon_r/\Gamma \lesssim 10^{-3}$ and $\delta\Gamma/\Gamma \lesssim 10^{-3}$ to achieve $\Delta_{2\pi} \lesssim \Delta_{4\pi}$. For bifluxon circuits, it may be difficult to limit the asymmetry $\delta\Gamma$, which is set by the fabrication of the tunnel junctions [154, 155] and cannot be tuned afterwards, unless SQUIDs are added to the design for the purpose. For semiconductor junctions, instead, a difficulty would be to maintain ϵ_r and $\delta\Gamma$ in such narrow ranges in the presence of charge noise. However, we argue that semiconductor junctions present a qualitative advantage relative to the bifluxon: stronger coupling between the weak link region and the superconducting leads can be achieved without sacrificing anharmonicity, namely without compromising the two-level approximation used in the model for the weak link [156]. As we explain below, the possibility to increase Γ without exiting the regime of validity of the model may be beneficial to find a parameter regime which offers more benevolent conditions to observe the 4π-dominated regime.

The duality derived in Sec. 3.4 is suggestive for the design of protected qubits. In the topological superconducting island, the regime $E_M = 0$ defines a parity-protected qubit [108]: as long as $E_J \gg E_C$, noise acting on the island can neither dephase nor flip the qubit encoded in the parity of the Majorana pair. In our inductive loop, a similar regime corresponds to the resonant condition $A_0 = 0$ together with the condition $2\pi^2 E_L \ll$

B_0 [7]. In this regime, noise in the loop cannot dephase or flip the qubit encoded in the fluxon parity of the loop. The former process is suppressed exponentially in the ratio $\sqrt{8B_0/(2\pi^2 E_L)}$.

From the theoretical point of view, both models discussed in Sec. 3.5 can be cast as a one-dimensional tight-binding model in which the nearest-neighbor hopping (E_M or A_0) can become smaller than the next-nearest neighbor hopping (E_J or B_0); the hopping represents tunneling of charge or flux depending on the side of the duality. When the nearest-neighbor hopping is set to zero but the next-nearest neighbor hopping is not, the one-dimensional lattice disconnects in two separate pieces, corresponding to "even" and "odd" sites of the lattice. Protected qubits can then be encoded in the parity degree of freedom: parity states are degenerate and have disjoint support. The degeneracy is broken by the inductive or charging energy, which assigns different energies to even and odd sites, but does not couple them [2]. With this general picture in mind, it becomes intuitive to see that the duality can be extended to other circuits – for instance, a transmon with both a $\cos(\phi)$ and a $\cos(2\phi)$ Josephson element – thus defining a sort of equivalence class of different models of protected superconducting qubits. Dualities of this type have also been discussed in Ref. [157].

From a practical point of view, an immediate problem with the protected regime of our model is the requirement for extreme smallness of E_L: to the best of our knowledge, the current record in the literature stands at $E_L/h \approx 65$ MHz [34], likely higher than what would be needed for the condition $2\pi^2 E_L \ll B_0$. A related issue is that the level spacing would be in the MHz range, requiring some active cooling to reach the quantum regime at accessible temperatures (milliKelvin scale). At low values of E_L – often reached via high-kinetic inductance thin-films with very low Cooper-pair densities – the occurrence of phase slips across the inductor, neglected here, may also have to be taken into account. A common strategy to minimize all the problems mentioned so far is to increase the quantum phase slip rates as well as the plasma frequency, essentially trying to maximize both Γ_A and E_C while keeping the ratio Γ_A/E_C constant and of order one. Using superconductors with a larger energy gap than Al in the resonant level junction would allow more room to increase

---

[2]When dealing with the Hamiltonian (3.25), one has to keep in mind that the boundary conditions (3.26) are twisted. After one makes a gauge transform to change the boundary conditions to periodic, the equilibrium charge n_g in the kinetic term is shifted differently for different parities.

Γ_A without exiting the tunneling limit. It is also essential to minimize the quasiparticle poisoning rate of the quantum dot (which is an analogue of the poisoning events of the Cooper pair box island in the bifluxon [7]), as our model (3.2) assumes even occupation numbers of the Andreev bound state.

Even then, the protected regime is fine-tuned by the need for the resonant condition to eliminate 2π quantum phase slips, which couple fluxons of different parity, breaking the parity protection. Possible circuit extensions that work around this fine-tuning problem were already discussed in the bifluxon proposal of Ref. [7] and could be adapted to semiconductor junctions as well.

Despite these obstacles, the existence of a protected regime, corroborated by the duality derived in this work, will make it interesting and rewarding to reach the hard-to-reach parameter regime in which the inductive energy becomes much smaller than the quantum phase slip rates.

3.6 Appendix: Definitions of the coefficients

In this Appendix, we give the explicit expressions for the coefficients $b_0, b_1, b_2, b_3, b_4, b_5$ used in the previous sections of this chapter. We introduce auxiliary definitions first:

$$u(\phi) = E_A(\phi)/\Gamma_A = \sqrt{1 - T\sin^2(\phi/2)}\,, \tag{3.27}$$

$$\mu(\phi) = \arcsin\sqrt{\frac{u(\varphi) - |r|}{u(\varphi) + |r|}}\,, \tag{3.28}$$

$$h = \frac{|r|}{(1 + |r|)\sqrt{1 - |r|}}\,, \tag{3.29}$$

$$k = \sqrt{\frac{1 - |r|}{1 + |r|}}\,. \tag{3.30}$$

Then b_0 and b_1 are defined in terms of elliptic integrals of the first and second kind, as follows:

$$b_0 = \lim_{\psi \to 0} \psi \; e^{\sqrt{2}h\left[2\Pi(\mu(\psi), k^{-2}, k) - (1-|r|)F(\mu(0), k)\right]} \tag{3.31}$$

$$b_1 = \sqrt{8}h\left[-F(\mu(0), k) + 2\Pi(\mu(0), 1, k)\right]\,. \tag{3.32}$$

For the rest of the coefficients, we have:

$$b_2 = \sqrt{\frac{T}{8}} \int_0^\pi \frac{(\pi^2 - \phi^2)d\phi}{\sqrt{1 - \sqrt{1 - T\cos^2 \phi/2}}}. \tag{3.33}$$

$$b_3 = \sqrt{2T}\, b_1 + \int_0^\pi \sqrt{1 + u(\phi)}d\phi \tag{3.34}$$

$$b_4 = \sqrt{\frac{T}{8}} \int_0^\pi \left[\frac{\phi(4\pi - \phi)}{\sqrt{1 - u(\phi)}} + \frac{4\pi^2 - \phi^2}{\sqrt{1 + u(\phi)}} \right] d\phi, \tag{3.35}$$

$$b_5 = \sqrt{\frac{T}{8}} \int_0^\pi \frac{d\phi}{\sqrt{1 + u(\phi)}}. \tag{3.36}$$

3.7 Appendix: Expressions for the low-energy Hamiltonian parameters

The expressions below are given in Ref. [22], where A_s, B_s are denoted $\delta_s^{2e}, \delta_s^{1e}$ and α_s, β_s are denoted $\beta_s^{2e}, \beta_s^{1e}$ respectively. We state them here for convenience. They have been derived using parabolic cylinder functions near the minima of the Josephson potential. The intermediate expressions (3.37), (3.39), (3.40) are different from [22], but the results for A_s, α_s and B_s, β_s are the same after the substitution of (3.39) into (3.37), (3.40). The 2π-tunneling amplitude and phase for a band s are given by:

$$A_s = \frac{w\omega_p}{z\pi} e^{-\tau_s}, \quad \alpha_s = \pi(s + 1) - \alpha \tag{3.37}$$

$$z = \frac{s!e^{s+1/2}}{(s + 1/2)^{s+1/2}\sqrt{2\pi}}, \tag{3.38}$$

with w and α as defined in the main text. Here, τ_s is some WKB integral that can be evaluated to:

$$e^{-\tau_s} = \frac{z\sqrt{2\pi}}{s!} \left(\frac{b_0^2 \omega_p}{4E_C} \right)^{s+\frac{1}{2}} \exp\left(-b_1 \frac{\omega_p}{E_C} \right). \tag{3.39}$$
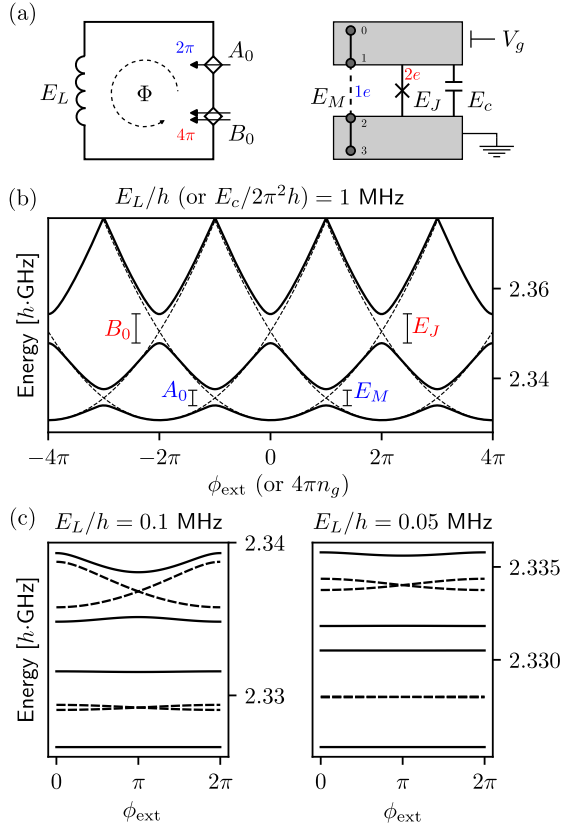
Note that the expression for $A_{s=0}$ coincides with Eq. (3.6) when $E_L/\omega_p \to 0$.

For 4π phase slips, there are two terms contributing to the overall amplitude B_s and phase β_s, which are defined by the equality:

$$B_s \cos(4\pi n + \beta_s) = \frac{(-1)^{s+1}\omega_p}{\pi z} e^{-\rho_s} e^{-\tau_s} \cos(4\pi n)$$

$$+ \frac{w^2 \omega_p}{2\pi^2 z^2} \log\left[\frac{b_0^2 \omega_p}{4E_C\left(s + \frac{1}{2}\right)}\right] e^{-2\tau_s} \cos(4\pi n - 2\alpha). \qquad (3.40)$$

Here ρ_s is another WKB integral, this time evaluating to

$$\rho_s = (b_3 - \sqrt{2T}b_1)\sqrt{\frac{\Gamma_A}{E_C}} - b_5(2s + 1). \qquad (3.41)$$

Figure 3.5. (a) Schematic illustration of the duality between a superconducting loop (left) with 2π and 4π phase slip elements A_0 and B_0 and a topological superconducting island (right) with $1e$ and $2e$ tunnel couplings E_M and E_J. The four grey dots on the right represent four Majorana zero modes, two on the island and two on the ground. Φ and V_g are the flux and voltage applied to the loop and island, corresponding to the tuning parameters $\phi_{\text{ext}} = 2\pi\,\Phi/\Phi_0$ and $n_g = CV_g/2e$. (b) Dispersion of the three lowest energy levels of the circuit as a function of flux, obtained from diagonalization of the $s = 0$ band Hamiltonian of Eq. (3.18). We set $E_C/h = 2.5$ GHz and $\Gamma/h = 5$ GHz, and $\epsilon_r/h = \delta\Gamma/h = 10$ MHz. In these conditions, the quantum phase slip parameters of Eq. (3.18) are $A_0 \approx 3.3$ MHz and $B_0/h \approx 6.7$ MHz. The dashed parabolas are the energies of uncoupled fluxons, which are dual to uncoupled charge states. Labels relate avoided crossings to model parameters on either side of the duality. (c) Flux dispersion of the energy levels of the circuit for lower values of E_L, illustrating the "transmon" regime. The solid lines are obtained for the same parameters as in panel (b), while the dashed lines are obtained at resonance: $\epsilon_r = \delta\Gamma = 0$. In this case, $A_0 = 0$ and energy levels gather in almost degenerate doublets. In panel (b), $B_0/(2\pi^2 E_L) \approx 0.3$, while in panel (c) $B_0/(2\pi^2 E_L) \approx 3.3$ and 6.6. Note that the vertical energy scale changes between plots, following the reduction in E_L.